

Scully-Lamb quantum laser model for parity-time-symmetric whispering-gallery microcavities: Gain saturation effects and non-reciprocity

Ievgen I. Arkhipov,¹ Adam Miranowicz,^{2,3} Omar Di Stefano,³ Roberto Stassi,³ Salvatore Savasta,^{4,3} Franco Nori,^{3,5} and Şahin K. Özdemir⁶

¹*RCPTM, Joint Laboratory of Optics of Palacký University and Institute of Physics of CAS, Faculty of Science, Palacký University, 17. listopadu 12, 771 46 Olomouc, Czech Republic*

²*Faculty of Physics, Adam Mickiewicz University, PL-61-614 Poznan, Poland*

³*Theoretical Quantum Physics Laboratory, RIKEN Cluster for Pioneering Research, Wako-shi, Saitama 351-0198, Japan*

⁴*Dipartimento di Scienze Matematiche e Informatiche,*

Scienze Fisiche e Scienze della Terra, Università di Messina, I-98166 Messina, Italy

⁵*Physics Department, The University of Michigan, Ann Arbor, Michigan 48109-1040, USA*

⁶*Department of Engineering Science and Mechanics, and Materials Research Institute (MRI), The Pennsylvania State University, University Park, Pennsylvania 16802, USA*

(Dated: May 20, 2022)

We use a non-Lindbladian master equation of the Scully-Lamb laser model for the analysis of light propagation in a parity-time symmetric photonic system composed of coupled active and passive whispering-gallery microresonators. Performing the semiclassical approximation, we obtain a set of two nonlinear coupled differential equations describing the time evolution of intracavity fields. These coupled equations are able to explain the experimentally-observed light non-reciprocity [Peng *et al.*, Nature Physics **10**, 394 (2014), Chang *et al.*, Nature Photonics **8**, 524 (2014)]. We show that this effect arises from the interplay between gain saturation in the active microcavity, intercavity coupling, and losses in the cavities. Additionally, using this approach, we study the effect of the gain saturation on exceptional points, i.e., exotic degeneracies in non-Hermitian systems. Namely, we demonstrate that the inclusion of gain saturation leads to a modification of the exceptional points in the presence of intense intracavity fields. The Scully-Lamb master equation for systems of coupled optical structures, as proposed and applied here, constitutes a promising tool for the study of quantum optical effects in coupled systems with losses, gain, and gain saturation.

I. INTRODUCTION

Recent years has witnessed an increasingly intense research effort to explore a class of non-Hermitian systems described by parity-time (\mathcal{PT}) symmetric Hamiltonians [1], (for reviews see [2, 3]). A system described by the Hamiltonian H is \mathcal{PT} -symmetric if it is invariant under the combined action of the parity \mathcal{P} and the time-reversal \mathcal{T} operators (i.e., H commutes with the \mathcal{PT} operator: $[H, \mathcal{PT}] = 0$) but not necessarily with the \mathcal{P} or \mathcal{T} operator alone. An important consequence of this is the necessary, but not sufficient, condition for \mathcal{PT} -symmetry: The complex potential $V(x) = V_r(x) + iV_i(x)$ of the Hamiltonian should satisfy $V(x) = V^*(-x)$, where the superscript $*$ denotes complex conjugation. In other words, the real part of the potential should be an even function of x , while its imaginary part should be an odd function of x , i.e., $V_r(x) = V_r(-x)$ and $V_i(x) = -V_i(-x)$. A \mathcal{PT} -symmetric system exhibits two very distinct phases: an unbroken \mathcal{PT} phase (also known as the exact- \mathcal{PT} regime), where the Hamiltonian supports real eigenvalues despite being non-Hermitian, and a broken \mathcal{PT} phase where some eigenvalues form complex conjugate pairs. The transition between these two phases takes place spontaneously as a result of parametric variation of the Hamiltonian. This *real-to-complex spectral phase transition* or the *\mathcal{PT} -phase transition point* exhibits all properties of an exceptional point (EP), which is defined as a singularity in the parameter space of a

non-Hermitian system at which two or more eigenvalues and their associated eigenvectors coalesce.

A decade after the ground-breaking work of Bender and Boettcher in 1998 which initiated the mathematical framework and fundamental understanding of \mathcal{PT} -symmetric systems [1], it was realized that \mathcal{PT} -symmetry and its breaking at an EP can be observed in photonics by imposing the necessary condition for \mathcal{PT} -symmetry on a complex optical potential, that is on the complex refractive index, $n(x) = n_r(x) + in_i(x)$, which leads to $n_r(x) = n_r(-x)$ and $n_i(x) = -n_i(-x)$ [4, 5]. Thus, an optical system with the \mathcal{PT} -symmetric potential has a symmetric index profile but an asymmetric gain/loss profile. Such a refractive index profile can be obtained in two coupled optical structures, such as waveguides or resonators: one having loss and the other having gain compensating the loss of the other. This discovery opened a very fertile research direction, where the interplay between gain, loss, and the strength of the coupling between them provides entirely new features and device functionalities [6–9]. In these non-Hermitian systems, with coupled loss and gain components, EPs can be observed by controlling (or tuning) the coupling strength to balance amplification (gain) and dissipation (loss). Thus, EPs can drastically alter the overall response of the system. This leads to a plethora of nontrivial phenomena [6–8], such as enhanced light-matter interactions [10–12], unidirectional invisibility [13, 14], lasers with enhanced mode selectivity [15, 16], low-power nonreciprocal light trans-

mission [17, 18], loss-induced lasing [19, 20], thresholdless phonon lasers [21, 22] to name a few. In parallel to these efforts in photonics, the concepts of \mathcal{PT} -symmetry have been put into use in electronics [23], optomechanics [21, 24, 25], acoustics [26, 27], plasmonics [28], and metamaterials [29]. More recently, there is a trend in investigating the features of \mathcal{PT} -symmetric quantum systems and the effect of \mathcal{PT} -symmetry and its breaking on the quantum states of light and the properties of quantum information [30–33].

Although \mathcal{PT} -symmetry and related concepts have their roots in quantum field theories, the experimental demonstrations and the majority of theoretical works are focused on *classical* systems, as in the example of two coupled optical microresonators: where the energy loss in one of them is compensated by the gain in the other, and the system is probed with light from a laser. In experiments, gain in such systems can be provided optically via parametric gain or Raman gain of the amplifying material; while the resonator is made from emitters or rare-earth ions embedded in it [17, 18]. The theoretical framework to analyze such systems relies on linearly-coupled rate equations of classical fields, where the gain and loss correspond to a different sign of the imaginary part of the complex frequencies (e.g., minus for gain and plus for loss, or vice versa) *without* a reference to how the gain and loss are generated. For example, the theoretical model, developed in Ref. [17], was linear without any nonlinearity, although the experimental results reported in that paper showed the presence of nonlinearity leading to nonreciprocal light transmission. Thus, the theoretical framework, applied there, failed to describe the observed non-reciprocity. On the other hand, in Ref. [18], closely following Ref. [17], a term was added phenomenologically (i.e., by hand) to the linear rate equations to include the effect of gain saturation, which provides the required nonlinearity for the nonreciprocal light transmission, *without* explicitly describing where this term comes from. One is also able to incorporate a nonlinear term in the rate equations to explain light non-reciprocity, but in the \mathcal{PT} -symmetric system of coupled waveguides [34], by resorting to a *semi-classical* Maxwell-Bloch approximation, where the dynamics is governed by a spatial variable, not time. On a different note, as the optical field is shifting from the classical to the quantum realm, it is important that the rate equations for the field operators are studied and the quantum-mechanical origins of gain and loss are properly described and incorporated into the models. Thus, a theoretical framework that addresses these concerns is highly desirable. Moreover, since the EP depends sensitively on the nonlinear coefficients, we can argue that having an ab-initio model is important for the question that this paper addresses. For this, we revisit the system, studied in Ref. [17], and later on in Ref. [18], of two coupled optical structures with loss, gain, and gain saturation by using a non-Lindbladian master equation originally derived for the Scully-Lamb laser model [35–37]. We apply this master equation for

the density operators of the optical fields in optical structures. Our approach explains (at a fundamental level) the results obtained in Refs. [17, 18] and explicitly describes the interplay of loss, gain, and gain saturation.

The paper is organized as follows. Section II contains the Hamiltonian of the system and the Scully-Lamb laser quantum master equation for the density operators of the optical fields. Section III presents the results, which include the rate equations of the field operators and their classical limit showing explicitly the presence of gain saturation nonlinearity and its effect on the eigenfrequencies and exceptional points of the system, as well as on the transmission spectra. Sections IV and V include a discussion of our results, future prospects, and a summary of the findings of this study.

II. LASER QUANTUM MASTER EQUATION FOR OPTICAL FIELDS IN COUPLED ACTIVE-PASSIVE MICRORESONATORS

Let us start from a description of the physical system that we would like to investigate in the Scully-Lamb laser model [35–37]. Our interest is focussed on the system which was experimentally studied first in Ref. [17] and later on in [18]. This system consists of two coupled whispering-gallery microresonators R_1 and R_2 , where R_1 is an active microresonator used for the amplification of optical fields, and R_2 is a passive microcavity, which only damps the propagating fields. We denote the Q -factors of the first and second microresonator as Q_1 and Q_2 , respectively. The schematic diagram of the described system is shown in Fig. 1. The coupling strength between the two microresonators is characterized by the real-valued parameter κ . Moreover, each microresonator is coupled to a different waveguide denoted as WG1 and WG2 with coupling constants γ_1 and γ_2 , respectively. The system shown in Fig. 1 is \mathcal{PT} -symmetric for balanced gain and loss. This is possible because the microresonators R_1 and R_2 become interchanged under the parity reflection \mathcal{P} , while loss and gain are interchanged under the time-reversal operation \mathcal{T} .

The active microresonator R_1 can be considered as a laser system with a laser gain medium. Naturally, in order to describe the dynamics of the electromagnetic field in the active laser microresonator one would resort to the quantum laser theory and its master equation [35–37].

The Hamiltonian of the coupled microresonators with one driving coherent field, which drives the active cavity, can be written as

$$\hat{H} = \sum_{k=1}^2 \hbar\omega_k \hat{a}_k^\dagger \hat{a}_k + i\hbar \left[\kappa \hat{a}_1 \hat{a}_2^\dagger + \epsilon \hat{a}_1 e^{i\omega_1 t} - \text{h.c.} \right], \quad (1)$$

where \hat{a}_k (\hat{a}_k^\dagger) is the boson annihilation (creation) operator of the mode $k = 1, 2$, with frequency ω_k ; and h.c. denotes Hermitian conjugate. Moreover, κ is the

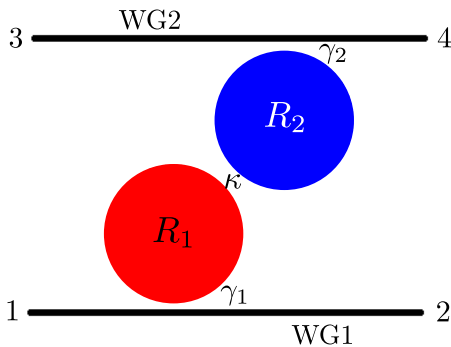


FIG. 1. Setup of the coupled active and passive whispering-gallery microresonators system studied here and in Ref. [17]. The active microresonator R_1 is coupled to the waveguide WG1 and also coupled to the passive resonator R_2 with coupling strengths γ_1 and κ , respectively. The coupling strength between the passive microresonator R_2 and the waveguide WG2 is denoted as γ_2 . The probe signal can be input from any port labelled from 1 to 4.

coupling strength between the microresonators, and ϵ is the coupling strength between the active cavity and the input signal driving field, with power P and frequency ω_l , which are related by $\epsilon \equiv \sqrt{\gamma_1 P / (\hbar \omega_l)}$. For the case when the passive cavity is driven, it is enough to swap the boson operator \hat{a}_1 with \hat{a}_2 in the last term of the Hamiltonian in Eq. (1).

By following the analysis of Yamamoto and Imamoglu [36], we consider our system as an ideal laser system in the Scully-Lamb laser model, which can be described by a non-Lindbladian master equation. This equation for the density operator $\hat{\rho}$ of the optical fields and for the Hamiltonian \hat{H} reads as follows (see Appendix A, for details):

$$\begin{aligned} \frac{d}{dt} \hat{\rho} = & \frac{1}{i\hbar} [\hat{H}, \hat{\rho}] + \left[\frac{A}{2} (\hat{a}_1^\dagger \hat{\rho} \hat{a}_1 - \hat{a}_1 \hat{a}_1^\dagger \hat{\rho}) \right. \\ & + \frac{B}{8} (\hat{\rho} (\hat{a}_1 \hat{a}_1^\dagger)^2 + 3 \hat{a}_1 \hat{a}_1^\dagger \hat{\rho} \hat{a}_1 \hat{a}_1^\dagger - 4 \hat{a}_1^\dagger \hat{\rho} \hat{a}_1 \hat{a}_1^\dagger \hat{a}_1) \\ & \left. + \sum_{i=1}^2 \frac{\Gamma_i}{2} (\hat{a}_i \hat{\rho} \hat{a}_i^\dagger - \hat{a}_i^\dagger \hat{a}_i \hat{\rho}) + \text{h.c.} \right], \end{aligned} \quad (2)$$

where the gain A and gain saturation B coefficients for the field in the active cavity are expressed as

$$A = \frac{2g^2 r}{Y^2}, \quad \text{and} \quad B = \frac{4g^2}{Y^2} A, \quad (3)$$

respectively. The parameter g stands for the coupling strength between the atoms of the gain medium and the optical field in the active cavity, Y is a decay rate of the atoms, and r accounts for the pump rate of the gain medium. In Eq. (2), the decaying rates for both cavities are denoted by ($i = 1, 2$)

$$\Gamma_i = C_i + \gamma_i, \quad \text{where} \quad C_i = \frac{\omega_i}{Q_i} \quad (4)$$

is the intrinsic loss of the i th cavity, and γ_i stands for the loss due to the coupling of the i th cavity to the i th waveguide.

We note that the derivation of the master equation in Eq. (2), as carried out in Appendix A, is based on two main assumptions: (i) the adiabatic elimination of the population in the gain medium of the active resonator, and (ii) the weak-gain-saturation regime, i.e., when the laser in the active cavity operates not far from the lasing threshold. The non-Lindbladian form of the master equation in Eq. (2), which is obtained within the fourth-order field approximation [36, 37], is due to quantum jump-operator terms, which account for gain saturation.

We also note that the master equation, given in Eq. (2), can be recast to the Lindbladian form as [38]:

$$\frac{d}{dt} \hat{\rho} = \frac{1}{i\hbar} [\hat{H}, \hat{\rho}] - \frac{1}{2} \sum_{i=1}^4 (\hat{L}_i^\dagger \hat{L}_i \hat{\rho} + \hat{\rho} \hat{L}_i^\dagger \hat{L}_i - 2 \hat{L}_i \hat{\rho} \hat{L}_i^\dagger), \quad (5)$$

where the Lindblad operators \hat{L}_i (for $i = 1, \dots, 4$) are defined as:

$$\begin{aligned} \hat{L}_1 = & \sqrt{A} \hat{a}_1^\dagger \left(1 - \frac{B}{2A} \hat{a}_1 \hat{a}_1^\dagger \right), \quad \hat{L}_2 = \frac{1}{2} \sqrt{3B} \hat{a}_1 \hat{a}_1^\dagger, \\ \hat{L}_3 = & \sqrt{\Gamma_1} \hat{a}_1, \quad \hat{L}_4 = \sqrt{\Gamma_2} \hat{a}_2. \end{aligned} \quad (6)$$

The Lindblad form in Eq. (5) is equivalent to the master equation (2) if the terms of second order in $B \hat{a}_1 \hat{a}_1^\dagger / (2A)$ are neglected in Eq. (5), which holds true for the weak gain saturation regime.

III. RESULTS

A. Rate equations

The master equation for the field operators, given in Eq. (2), and the Hamiltonian in Eq. (1), yield the rate equations for the averaged boson operators \hat{a}_1 and \hat{a}_2 . Namely, by using the formula

$$\frac{d}{dt} \langle \hat{a}_j \rangle = \text{Tr} \left[\hat{a}_j \frac{d}{dt} \hat{\rho} \right], \quad j = 1, 2, \quad (7)$$

and utilizing the cyclic property of the trace operation, after substituting Eq. (2) in Eq. (7), we obtain

$$\begin{aligned} \frac{d}{dt} \langle \hat{a}_1 \rangle = & -i\omega_1 \langle \hat{a}_1 \rangle + \frac{G_1}{2} \langle \hat{a}_1 \rangle - \kappa \langle \hat{a}_2 \rangle - \frac{B}{2} \langle \hat{a}_1^\dagger \hat{a}_1 \hat{a}_1 \rangle, \\ & - \epsilon \exp(-i\omega_l t), \\ \frac{d}{dt} \langle \hat{a}_2 \rangle = & -i\omega_2 \langle \hat{a}_2 \rangle - \frac{\Gamma_2}{2} \langle \hat{a}_2 \rangle + \kappa \langle \hat{a}_1 \rangle, \end{aligned} \quad (8)$$

where $G_1 = A - \Gamma_1 - \frac{7}{4}B$.

As one can see, the rate equations, given in Eq. (8) for the averaged quantum amplitudes, are nonlinear due to the presence of the gain saturation in the active cavity, i.e., the term $(B/2) \langle \hat{a}_1^\dagger \hat{a}_1 \hat{a}_1 \rangle$ represents the nonlinearity.

B. Classical Limit

In the classical limit, i.e., in the case of large intensities of the fields, the quantum field operators can be represented by c -number amplitudes as $\hat{a}_i \rightarrow \langle \hat{a}_i \rangle \equiv a_i$. Then the rate equations in Eq. (8) can be rewritten in the classical limit as

$$\begin{aligned} \frac{d}{dt}a_1 &= -iw_1a_1 + \frac{G_1}{2}a_1 - \kappa a_2 - \frac{B}{2}|a_1|^2a_1 - \epsilon \exp(-i\omega t), \\ \frac{d}{dt}a_2 &= -iw_2a_2 - \frac{\Gamma_2}{2}a_2 + \kappa a_1, \end{aligned} \quad (9)$$

where the term $\frac{B}{2}|a_1|^2a_1$ represents the nonlinearity due to gain saturation. By substituting $a_k = A_k(t) \exp(-i\omega t)$ into Eq. (9), one arrives at

$$\begin{aligned} \frac{d}{dt}A_1 &= i\Delta A_1 + \frac{G_1}{2}A_1 - \kappa A_2 - \frac{B}{2}|A_1|^2A_1 - \epsilon, \\ \frac{d}{dt}A_2 &= i\Delta A_2 - \frac{\Gamma_2}{2}A_2 + \kappa A_1, \end{aligned} \quad (10)$$

where $\Delta = \omega - \omega_c$ is the frequency-detuning parameter, and we assumed that the frequency of the driving coherent field is $\omega_l = \omega$, and the frequencies of the cavities are the same, $\omega_1 = \omega_2 = \omega_c$. We note that when the input driving field enters the passive cavity from port 4 in Fig. 1, then the term $(-\epsilon)$ would appear in the second equation (instead of the first) in Eq. (10). Importantly, in the semiclassical approximation, the coupling constant ϵ can be expressed via the complex amplitude A_{in} of the input driving field as $\epsilon \equiv \sqrt{\gamma_j}A_{\text{in}}$, for $j = 1, 2$. Nevertheless, for convenience, we will keep the current notation for the input driving field via ϵ , because it shares the same dimensionality with the other parameters describing the system. Moreover, by keeping this notation it will be more transparent and easier for us to compare the semiclassical and fully quantum approaches in related future research. In what follows, we will always recall the connection between the driving coupling constant ϵ and the input driving field amplitude A_{in} to avoid any confusion.

It is clearly seen from Eq. (10) that the rate equations simplify to a linear form if the gain saturation in the active laser cavity are neglected.

We note that in the semiclassical Maxwell-Bloch picture, which is widely used for describing the characteristic \mathcal{PT} -symmetric properties of classical optical fields, one can introduce gain saturation via a modified gain coefficient A for the field A_1 in the active cavity as $A \rightarrow A/(1 + |A_1|^2/|A_s|^2)$ in Eq. (10) for $B = 0$, where $|A_s|^2$ is the gain saturation threshold [18]. In this case, by decomposing this modified gain coefficient A in a Taylor series (up to the first order in $|A_1|^2/|A_s|^2 \ll 1$, which is justified in the weakly saturated regime), one obtains a one-to-one correspondence between the semiclassical Maxwell-Bloch picture and the semiclassical Scully-Lamb laser model for the optical fields in Eq. (10) by setting $B = A/|A_s|^2$. Nevertheless, compared to the Maxwell-Bloch picture, where the gain saturation term is introduced phenomenologically, the semiclassical Scully-Lamb

laser theory explains gain saturation not only qualitatively, but also quantitatively, via the laser system parameters given in Eq. (3).

We also note that a set of nonlinear equations, similar to Eq. (10), can be obtained within the semiclassical Maxwell-Bloch approximation for \mathcal{PT} -symmetric coupled waveguides [34]. Nonetheless, there are two main differences with respect to Ref. [34]. The first is that we consider the case of coupled resonators instead of coupled waveguides. In our case, feedback effects and two different kinds of losses (i.e., input-output and intrinsic losses) are considered. Second, even if we apply the semiclassical approximation, our theory is based on a fully quantum approach, which can be useful to investigate quantum effects and quantum noise.

C. Eigenfrequencies in the steady-state and exceptional point

In the steady state, by considering $\gamma_1 = \gamma_2 = \gamma$ for symmetry reasons, we find from Eq. (10) that:

$$\begin{aligned} \left(i\Delta + \frac{G'_1}{2}\right)A_1 - \kappa A_2 &= \epsilon, \\ \left(i\Delta - \frac{\Gamma_2}{2}\right)A_2 + \kappa A_1 &= 0, \end{aligned} \quad (11)$$

where $G'_1 = G_1 - B|A_1|^2$. Because the system of equations in Eq. (11) is written for the complex fields A_j , we can incorporate the real steady-state intensity $|A_1|^2$ into the prefactor G'_1 . One can obtain the eigenvalues of the system, given in Eq. (11), by setting the driving field to zero ($\epsilon = 0$). Defining the vector $\alpha = (A_1, A_2)^T$, we can rewrite Eq. (11) as follows

$$i\frac{d\alpha}{dt} = M\alpha, \quad (12)$$

with the evolution matrix

$$M = \begin{pmatrix} -\Delta + i\frac{G'_1}{2} & -i\kappa \\ i\kappa & -\Delta - i\frac{\Gamma_2}{2} \end{pmatrix}. \quad (13)$$

For the case when gain and losses are balanced, i.e., when $G'_1 = \Gamma_2$ holds, the evolution matrix M , given in Eq. (13), becomes \mathcal{PT} -symmetric, i.e., $[M, \mathcal{PT}] = 0$, with the parity operator $\mathcal{P} = \begin{pmatrix} 0 & 1 \\ 1 & 0 \end{pmatrix}$ and \mathcal{T} performing complex conjugation.

The characteristic equation of the matrix M is

$$\left(\Delta - i\frac{G'_1}{2}\right)\left(\Delta + i\frac{\Gamma_2}{2}\right) - \kappa^2 = 0, \quad (14)$$

from which we find the formal solution for the eigenfrequencies, as follows

$$\Delta_{\pm} = i\frac{G'_1 - \Gamma_2}{4} \pm \sqrt{4\kappa^2 - \frac{1}{4}(G'_1 + \Gamma_2)^2}. \quad (15)$$

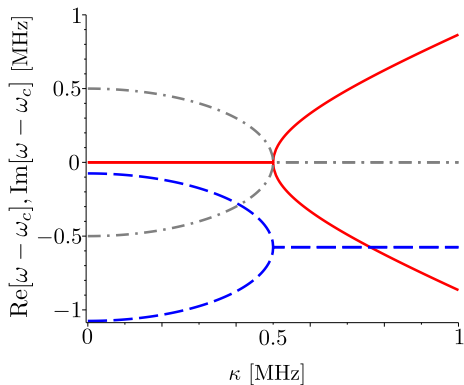


FIG. 2. Real part, $\text{Re}[\omega]$, (red solid curve) and imaginary part, $\text{Im}[\omega]$, (blue dashed curve) of the eigenfrequencies of the supermodes, as a function of coupling κ at the \mathcal{PT} -symmetry condition $A - C_1 - C_2 - BI_1 = 0$. The exceptional point does not depend on gain saturation. We have chosen $C_2 = 1$ MHz, $\gamma = 1.15$ MHz. In addition, we show $\text{Re}[\omega]$ (red solid curve, which overlaps with the other red curve) and $\text{Im}[\omega]$ (gray dash-dotted curve) of the eigenfrequencies of the supermodes when the input-output losses are not considered. Here ω_c stands for the cavities resonance.

By recalling that $\Delta_{\pm} = \omega_{\pm} - \omega_c$, we obtain

$$\omega_{\pm} = \omega_c + \frac{i}{4} (A - C_1 - C_2 - BI_1 - 2\gamma) \pm \frac{1}{2} \sqrt{4\kappa^2 - \frac{1}{4} (A - C_1 + C_2 - BI_1)^2}, \quad (16)$$

where $I_1 = |A_1|^2$ is the dimensionless intensity of the field in the active cavity in the steady-state, and which is by itself a function of the frequency ω (for the solutions of the steady-state intensity I_1 , see Section III E). The solutions in Eq. (16) give the energy eigenspectra of the system, i.e., the eigenvalues of the system Hamiltonian, which determine the evolution matrix M .

We note again that, in reality, the loss rates γ_i , arising from the coupling with the input-output channels, are not true losses, because these describe the energy transfer from the system to the output (or from the input to the system). Hence, the concept of the *effective* \mathcal{PT} -symmetry in our system with balanced gain and loss, can be expressed as

$$A - C_1 - C_2 - BI_1 = 0. \quad (17)$$

This is valid because the system is \mathcal{PT} -symmetric regardless of how it is probed (i.e., waveguides in the coupled resonator systems are used only to probe the system). When the condition, given in Eq. (17), is satisfied we find from Eq. (16) that:

$$\omega_{\pm}^{\text{PT}} = \omega_c - i\frac{\gamma}{2} \pm \frac{1}{2} \sqrt{4\kappa^2 - C_2^2}. \quad (18)$$

Note that, when changing the input signal ϵ (and hence the resulting steady-state intensity I_1), one has to adjust

the losses correspondingly in order to satisfy the \mathcal{PT} -symmetry condition.

The analysis of the frequency spectrum, given in Eqs. (16) and (18), provides two different regimes, or so-called *unbroken* and *broken* \mathcal{PT} -symmetry phases, depending on the sign of the expression under the square-root sign. In the unbroken \mathcal{PT} -symmetry phase, the expression under the root is positive (that is, $\kappa > \frac{C_2}{2}$), and there are always two supermodes with non-degenerate real frequencies ω_{\pm} that propagate in the system. Note that this is true for the system itself, where the coupling loss γ (which is not inherent to the system of coupled resonators) is zero (i.e., $\gamma = 0$). In the broken \mathcal{PT} -symmetry phase, that expression is negative (that is, $\kappa < C_2/2$), and the real spectrum becomes degenerate, indicating that the system displays two modes with the same resonance frequency but with different decay rates. The transition between these two regimes takes place at an EP given by

$$\kappa_{\text{EP}} = \frac{C_2}{2}. \quad (19)$$

In Fig. 2 we show the real and imaginary parts of the eigenfrequencies of the supermodes. As expected by the inspection of Eq. (19), the EP at $\kappa = \kappa_{\text{EP}}$ does not depend on the field intensity. For $\kappa > \kappa_{\text{EP}}$, we observe that the imaginary part is different from zero. This is due to the contributions of the loss rates γ_i arising from the coupling with the input-output channels. The gray dash-dotted curve in Fig. 2 describes the imaginary parts of the complex eigenfrequencies, when the input-output coupling losses are neglected (i.e., $\gamma = 0$).

We now consider the case, where the \mathcal{PT} -symmetry condition is achieved at low input rates, so the gain saturation effects are negligible ($BI_1 \simeq 0$). In this case, as for the \mathcal{PT} -symmetry condition, we can use Eq. (17) calculated for $I_1 = 0$:

$$A - C_1 - C_2 = 0. \quad (20)$$

If the input drive is increased without adjusting the other parameters (κ and C_i), the \mathcal{PT} -symmetry condition is not satisfied any more. We will investigate the effect of gain saturation on the spectral properties of the considered \mathcal{PT} -symmetric system, which is usually studied without the inclusion of gain saturation. Thus, hereafter, we assume that the \mathcal{PT} -symmetric condition is given in Eq. (20). The condition for the exceptional point becomes [see Eq. (16)]:

$$\kappa_{\text{EP}} = \frac{1}{4} |A - C_1 + C_2 - BI_1| = \frac{1}{4} |2C_2 - BI_1|. \quad (21)$$

From inspection of Eq. (21), we observe that, in this case, the EP changes when the steady-state field intensity increases in the active cavity (see Fig. 3). In particular, as an example, in Fig. 3 we plot the real and imaginary parts of the eigenfrequencies of the supermodes for the linear [Fig. 3(a)] and nonlinear [Figs. 3(b)–(d)] regimes

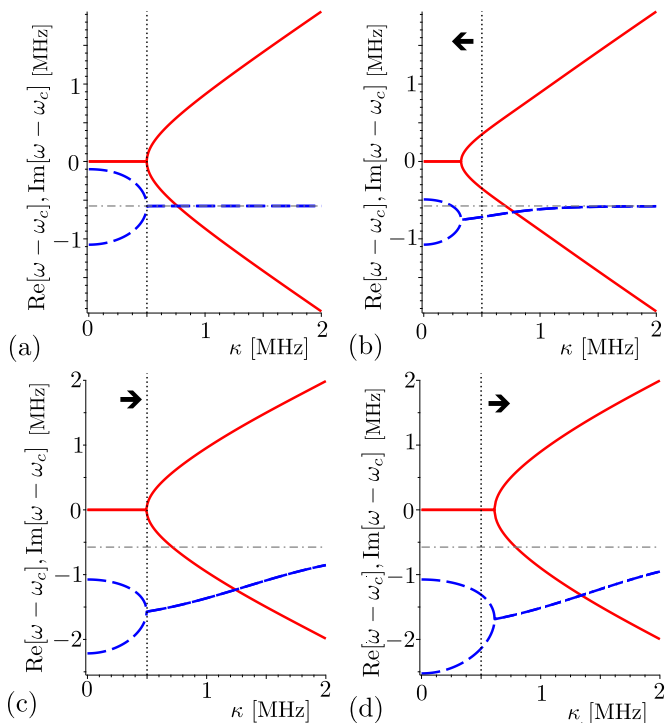


FIG. 3. Real part, $\text{Re}[\omega]$, (red solid curve) and imaginary part, $\text{Im}[\omega]$, (blue dashed curve) of the eigenfrequencies of the supermodes as a function of the coupling κ under the \mathcal{PT} -symmetry condition $A - C_1 - C_2 = 0$ (i.e., excluding the gain saturation term BI_1) for different values of the coupling coefficient ϵ of the driving field to a microresonator (see Fig. 1). It is seen that exceptional point depends on gain saturation. (a) The linear regime with $B = 0.05$ Hz and $\epsilon = 1$ MHz; and (b, c, d) the nonlinear regime according to Eq. (22) with $B = 0.05$ Hz with (b) $\epsilon = 2$ GHz, (c) $\epsilon = 20.5$ GHz, and (d) $\epsilon = 25$ GHz. The observed inclination of the imaginary part of the eigenfrequencies (blue dashed curve) towards negative values near the EP indicates an additional loss due to gain saturation caused by stronger driving fields. We assumed a passive cavity loss of $C_2 = A - C_1 = 1$ MHz, an active cavity gain of $A = 301$ MHz, and a waveguide-microresonator coupling strength of $\gamma = 1.15$ MHz. The vertical black dashed line denotes the EP κ_{EP} for the linear system, when the gain saturation term $BI_1 = 0$. The horizontal gray dash-dotted line denotes the converging value $(\gamma/2)$ for the imaginary part of the eigenfrequencies (blue dashed curve) for large κ . The condition $BI_1/A \ll 1$ for a weak saturation is always satisfied for all the cases corresponding to panels (a)–(d) (see also Appendix B).

for different values of the driving-field coupling ϵ when driving the system at a resonant frequency ω_c .

In the linear regime, the gain saturation term BI_1 is either exactly zero or negligible compared to the system parameters A and C_i ; thus, the behavior of the EP is identical to that presented in Fig. 2 [see also Figs. 3(a) and 4(a)]. The same conclusion applies when the driving field is far away from the resonance ω_c , as in that case, the steady-state intensity also tends to zero.

An interesting situation arises when the gain satu-

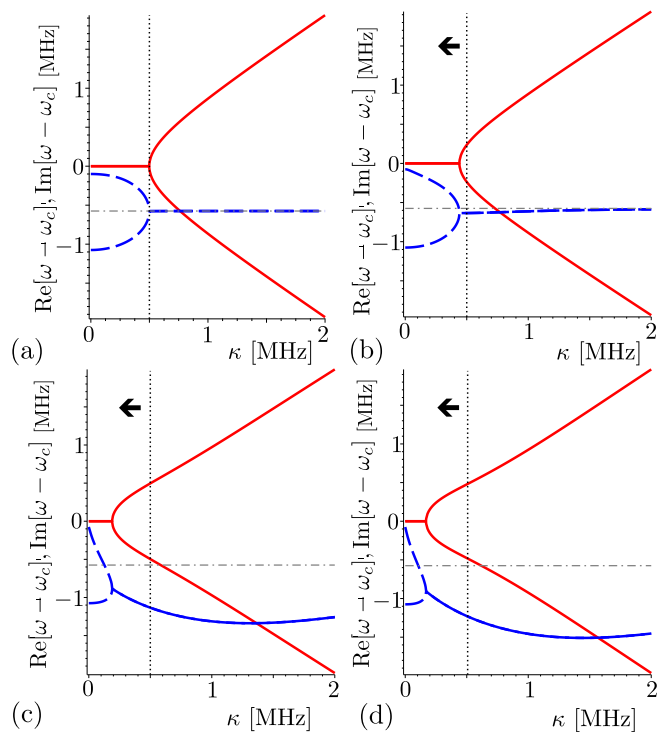


FIG. 4. Real part, $\text{Re}[\omega]$, (red solid curve) and imaginary part, $\text{Im}[\omega]$, (blue dashed curve) of the eigenfrequencies of the supermodes as a function of the coupling κ under the \mathcal{PT} -symmetry condition $A - C_1 - C_2 = 0$ (i.e., excluding the gain saturation term BI_1) for different values of the coupling coefficient ϵ when the driving field drives the passive cavity (see Fig. 1). The parameters used here are the same as in Fig. 3.

ration term BI_1 becomes comparable with the passive cavity loss C_2 . However, at the same time, it is much less than the gain coefficient A in the active cavity, i.e., $BI_1 \ll A$, so the weakly saturated regime still holds and the validity of the master equation in Eq. (2) remains. This also implies that $C_1 \gg C_2$. In this case, the system starts exhibiting some nonlinear features in its eigenspectrum. In short, the described condition can be written as

$$BI_1 \approx C_2 \ll A \approx C_1. \quad (22)$$

In what follows, we always call the system to be in the *nonlinear* \mathcal{PT} -symmetric regime, whenever *both* conditions, given in Eqs. (20) and (22), are satisfied. In that case, one can observe that the critical value of κ_{EP} significantly changes depending on the gain saturation term BI_1 . Moreover, the steady-state intensity I_1 in the active cavity by itself becomes dependent on the direction of the propagation of the driving field, i.e., on whether the driving field is coupled to the active (from port 1 to port 4) or the passive cavity (from port 4 to port 1) [see Fig. 1]. Consequently, the gain saturation term BI_1 also depends on the driving-field direction.

When the input driving field is coupled to the active

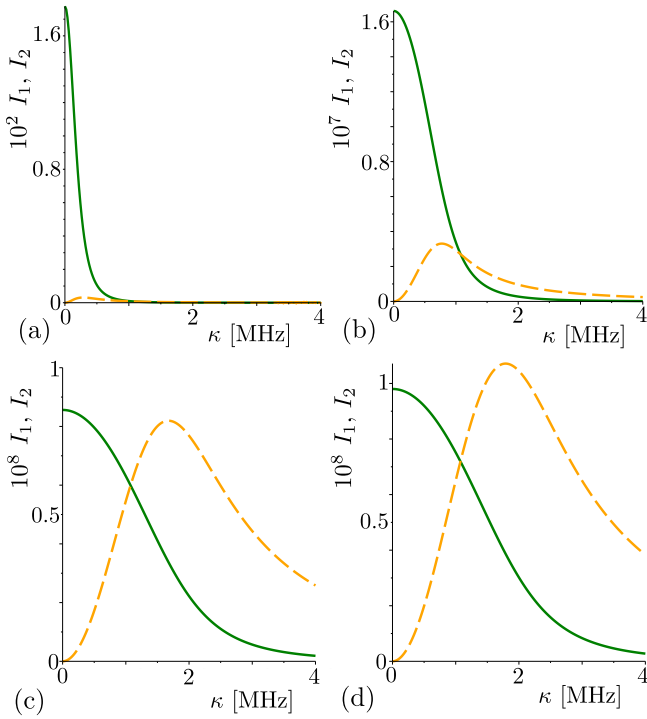


FIG. 5. Dimensionless steady-state intensities I_1 (green solid curve) and I_2 (yellow dashed curve) in the active and passive cavities, respectively, as a function of the inter-cavity coupling κ for the driving field propagating in the direction $1 \rightarrow 4$ (see Fig. 1). The panels (a) – (d) are obtained for different values of the driving field coupling ϵ and correspond to the panels in Fig. 3.

cavity, it can experience a significant gain saturation for large input intensities, and, as a result, its losses increase. This especially happens when one decreases the inter-cavity coupling κ . In the latter case, the strong signal field becomes localized in the active resonator, before being transferred to the lossy passive cavity. This leads to the gain decrease of the intense driving field due to gain saturation, and, therefore, to the observed signal-field losses (see blue dashed curve in Fig. 3). Moreover, when the losses induced by the gain saturation become comparable to the losses in the passive cavity (i.e., when $BI_1 \approx C_2$), then the critical value of κ_{EP} first decreases and then increases when increasing the intensity of the input field (see Fig. 3). As Eq. (21) implies, this shift of κ_{EP} can be explained by the interplay between losses in the passive cavity and losses induced by gain saturation in the active resonator. Namely, by increasing the gain saturation term BI_1 (i.e., by increasing the input signal) in the proximity of C_2 in Eq. (21), the critical value κ_{EP} first decreases, when $BI_1 \leq C_2$, and then increases, when $BI_1 \geq C_2$.

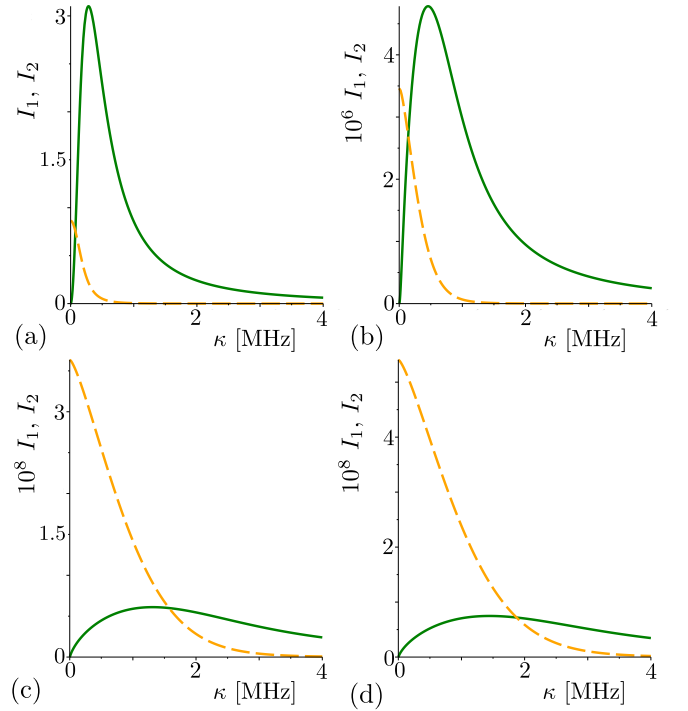


FIG. 6. Dimensionless steady-state intensities I_1 (green solid curve) and I_2 (yellow dashed curve) in the active and passive cavities, respectively, as a function of the inter-cavity coupling κ for the driving field propagating in the direction $4 \rightarrow 1$ (see Fig. 1). The panels (a) – (d) are obtained for different values of the driving-field coupling ϵ and correspond to the panels of Fig. 4.

D. Non-reciprocity of light propagation

Another important result of our work is the theoretical microscopic *prediction of non-reciprocity of the propagating light*. Specifically, in broken \mathcal{PT} -symmetry phase, i.e., when $\kappa < \kappa_{EP}$, the signal field can experience smaller losses for smaller values of κ , when the driving field propagates in the direction $4 \rightarrow 1$, in comparison to the case when it propagates in the opposite direction $1 \rightarrow 4$ (see Fig. 4). This stems from the fact, that when the strength of the input signal field is increasing, by decreasing the inter-cavity coupling κ , the driving field experiences large losses in the passive cavity before passing into the active resonator. Now, because the initially strong input signal field is strongly damped by the passive resonator, it enters the active cavity having an intensity which is not sufficient to induce gain saturation. As such, the propagating field in the active cavity can even undergo notable amplification before being detected at port 1. As a result, the critical values of κ_{EP} only decrease when increasing the intensity of the input signal field, since the propagating field cannot reach high intensity in the active cavity to make the term BI_1 larger than C_2 in Eq. (21) (see also Fig. 4).

We plotted Figs. 5–7 to demonstrate the aforementioned

tioned asymmetry of the steady-state intensities in both cavities depending on the propagation direction of the resonant signal field. As it follows from Fig. 7, for very small values of $\kappa < \kappa_{\text{EP}}$, the field intensity in the active cavity for the direction $4 \rightarrow 1$ can be two or three orders of magnitude larger than the intensity in the passive cavity for the opposite propagation direction $1 \rightarrow 4$. As a consequence, this asymmetric property can lead to the observation of non-reciprocal light behavior for small κ . Therefore, the non-reciprocity of light propagation, as experimentally demonstrated in, e.g., Ref. [17], arises from the combination of loss, gain, and gain saturation. Specifically, owing to the saturation effects, the gain experienced by the signal entering the amplifying cavity strongly depends on its intensity. We would like to stress again that the input signal with a large intensity undergoes a much lower amplification with respect to a weaker signal due to gain saturation. Hence, feeding the gain cavity with a quite strong field gives rise to a modest amplification (see also Fig. 8). This signal is finally strongly absorbed by the lossy cavity, before being detected. By contrast to this, if the same signal is first sent to the lossy cavity, then it is strongly absorbed before entering the gain cavity. Such a small signal does not saturate the gain medium and is strongly amplified before detection.

As Figs. 3 and 4 also indicate, in unbroken \mathcal{PT} -symmetry phase, for large values of the intercavity coupling $\kappa \gg \kappa_{\text{EP}}$, the system exhibits a linear character, regardless of both strengths of the input signal field and the propagation direction ($1 \rightarrow 4$ and $4 \rightarrow 1$). Indeed, in this case, the coupling κ between two microcavities becomes large enough, enabling the input signal fields to freely propagate in either direction. Hence, there is no localization of the fields in the system, and, thus, there is no observed nonlinearity due to gain saturation.

E. Transmission spectra

Here we focus on the spectral properties of the driving fields that propagate through the system.

By rewriting the complex amplitudes A_k of the fields [as in Eq. (10)] as $A_k = |A_k| \exp(i\phi_k)$, one arrives at a cubic equation for the field intensity I_1 in the active cavity in the steady state (see Appendix B, for details):

$$\lambda_1 I_1^3 + \lambda_2 I_1^2 + \lambda_3 I_1 + \lambda_4 = 0, \quad (23)$$

with coefficients λ_i defined as:

$$\begin{aligned} \lambda_1 &= \frac{B^2}{4}, & \lambda_2 &= BF, & \lambda_4 &= -\epsilon^2, \\ \lambda_3 &= F^2 + \Delta^2 (f - 1)^2, & F &= \frac{1}{2} (f\Gamma_2 - G_1), \end{aligned} \quad (24)$$

where $f = 4\kappa^2 / (\Gamma_2^2 + 4\Delta^2)$. Equation (23) has only one real solution (see Appendix B, for details), when its discriminant is negative, which is always the case when, e.g., $A \approx \Gamma_1$ regardless of Γ_2 and κ .

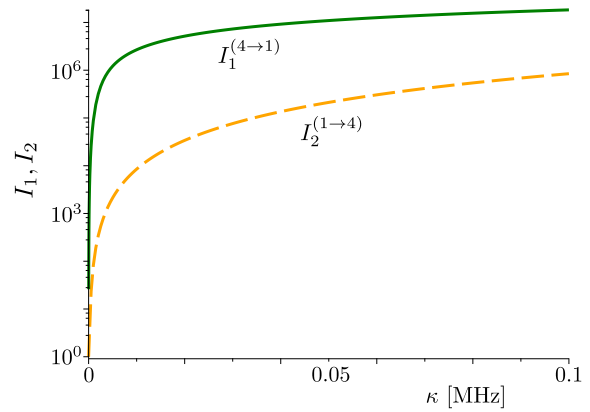


FIG. 7. Dimensionless steady-state intensity $I_1^{(4 \rightarrow 1)}$ (green solid curve) in the active cavity for the driving field propagating in the direction $4 \rightarrow 1$ from Fig. 6(d), and the steady-state intensity $I_2^{(1 \rightarrow 4)}$ (yellow dashed curve) in the passive cavity for the driving field propagating in the direction $1 \rightarrow 4$ from Fig. 5(d) for lower values of κ . For the broken- \mathcal{PT} -symmetric phase in the nonlinear regime for small values of $\kappa < \kappa_{\text{EP}}$, the steady-state intensity $I_1^{(4 \rightarrow 1)}$ is two-three orders of magnitude larger than $I_2^{(1 \rightarrow 4)}$, implies nonreciprocal light propagation.

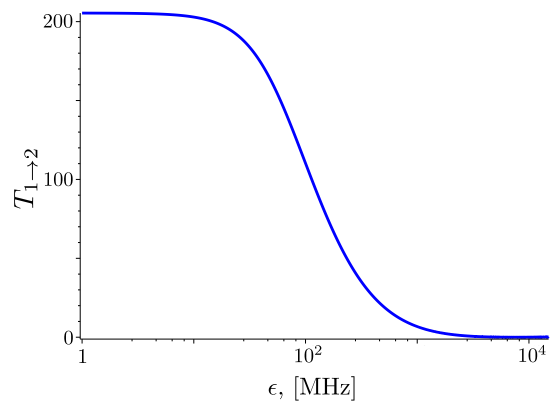


FIG. 8. Transmissivity $T_{1 \rightarrow 2}$ of light as a function of the input driving field signal ϵ , with resonant driving frequency $\omega = \omega_c$, when there is no passive cavity in the system, i.e., $\kappa = 0$ (see Fig. 1). The driving field coupling constant ϵ is related to the amplitude A_{in} of the input signal via the expression $\epsilon = \sqrt{\gamma_1} A_{\text{in}}$. The plot presents the gain behaviour in the active cavity versus the intensity of the input signal field. With increasing strength of the input signal ϵ , the gain (represented by the transmissivity $T_{1 \rightarrow 2}$) of the signal field steadily decreases due to gain saturation. The remaining parameters used here are the same as in Fig. 3. For details, regarding the transmission coefficients, see also Sec. III E.

The transmission spectrum can be calculated as follows

$$T(\omega) = \left| \frac{A_{\text{out}}}{A_{\text{in}}} \right|^2. \quad (25)$$

To obtain the transmission spectrum $T_{1 \rightarrow 4}(\omega)$ at port 4 when sending the signal from port 1, one needs to know the expressions for the corresponding input-output fields.

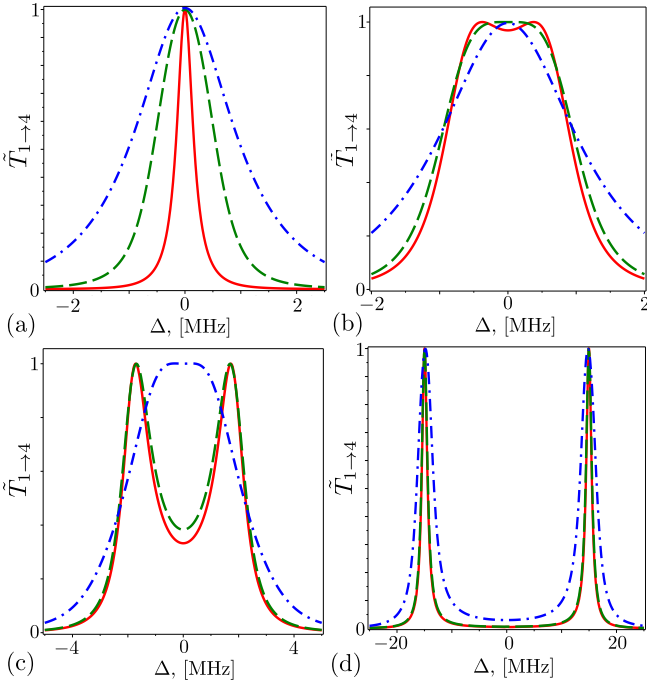


FIG. 9. Normalized transmission spectrum $\tilde{T}_{1 \rightarrow 4} = T_{1 \rightarrow 4}(\Delta)/\max[T_{1 \rightarrow 4}(\Delta)]$ versus detuning $\Delta = \omega - \omega_c$, where $T_{1 \rightarrow 4}(\Delta)$ is given in Eq. (26) (see also Fig. 1, for details), for different values of the intercavity coupling κ : (a) $\kappa = 0.3$ MHz, (b) $\kappa = 0.85$ MHz, (c) $\kappa = 1.88$ MHz and (d) $\kappa = 15$ MHz with the \mathcal{PT} -symmetry condition $A - C_1 - C_2 = 0$ (excluding the gain saturation term BI_1). The linear regime with $B = 0.05$ Hz and $\epsilon = 1$ MHz (red solid curve); the nonlinear regime, according to Eq. (22), with $B = 0.05$ Hz and $\epsilon = 2$ GHz (green dashed curve) and $\epsilon = 20.5$ GHz (blue dash-dotted curve). Assuming the passive cavity loss $C_2 = 1$ MHz, the active cavity gain $A = 301$ MHz, and the waveguides coupling with both cavities is $\gamma = 1.15$ MHz. The transmission spectra in panel (a) and panel (d) exhibit Lorentzian line shapes, when the system is well below or above from the EP, respectively [39]. On the contrary, in panel (b) and panel (c), the transmission spectra have squared Lorentzian line shapes, which is a signature of the occurrence of EPs [39–41].

The output field at port 4 is found as $A_{\text{out}} = \sqrt{\gamma_2}A_2$. The input driving field sent from port 1 can be expressed, as $A_{\text{in}} = \epsilon/\sqrt{\gamma_1}$, where, again, ϵ is the coupling strength between input driving field and microresonator (Fig. 1). By rewriting the field A_2 via A_1 and using Eq. (10), one finally obtains

$$T_{1 \rightarrow 4}(\Delta) = \frac{4\kappa^2\gamma_1\gamma_2}{\epsilon^2(\Gamma_2^2 + 4\Delta^2)}I_1. \quad (26)$$

The same analysis can be carried out for the case when the driving coherent field is sent from port 4, and the signal is detected at port 1. In that case, one obtains the same cubic equation for the field intensity I_1 , as in Eq. (23), but with different λ_k ; $k = 1, \dots, 4$ (see Appendix B). The expression for the transmission spectra

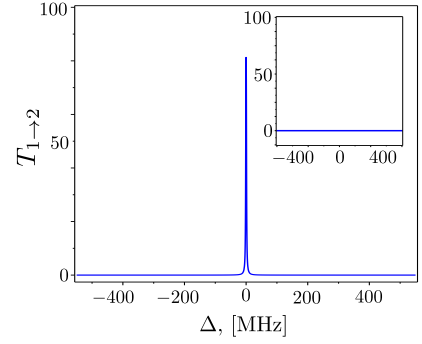


FIG. 10. Transmission spectrum $T_{1 \rightarrow 2}$ assuming that there is coupling only between the WG_1 and the active microcavity R_1 ; the active cavity gain is $A = 20.4$ MHz, and the power of the driving field is $P = 100$ nW. The inset shows the transmissivity when the power of the driving field is $P = 0$. Here and in the graphs below, the resonance wavelength of both cavities is set as $\lambda_c = 1550$ nm. Moreover, we assume that all losses in both cavities are encompassed by the waveguides couplings, i.e., $\Gamma_i = C_i + \gamma_i \approx \gamma_i$, $i = 1, 2$, and their values are fixed along with the gain saturation coefficient, i.e., $\gamma_1 = 25$ MHz, $\gamma_2 = 10$ MHz, and $B = 0.1$ Hz. This figure qualitatively reproduces the experimentally-obtained Fig. 1(f) in Ref. [17].

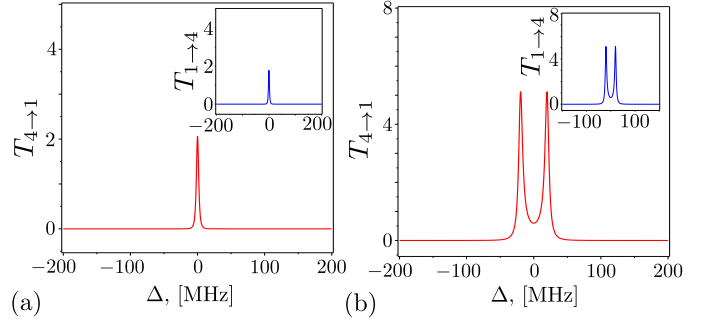


FIG. 11. Transmission spectrum $T_{4 \rightarrow 1}$ (red curve) and $T_{1 \rightarrow 4}$ (blue curve inside in the captions) in the linear regime when: (a) $A = 21$ MHz, $\kappa = 1$ MHz, and $P = 100$ nW; (b) $A = 21$ MHz, $\kappa = 20$ MHz, and $P = 100$ nW. This figure qualitatively reproduces the experimentally-obtained Fig. 3 in Ref. [17]

$T_{4 \rightarrow 1}(\omega)$ then attains the following form

$$T_{4 \rightarrow 1}(\omega) = \frac{\gamma_1\gamma_2}{\epsilon^2}I_1. \quad (27)$$

Similarly, the transmission spectrum $T_{1 \rightarrow 2}$ can be found using the input-output relation: $A_{\text{out}} = A_{\text{in}} + \sqrt{\gamma_1}A_1$ (see Appendix B, for details).

As an example, in Fig. 9 we plot the normalized transmission spectrum $\tilde{T}_{1 \rightarrow 4} = T_{1 \rightarrow 4}(\Delta)/\max[T_{1 \rightarrow 4}(\Delta)]$ for the \mathcal{PT} -symmetric condition $A - C_1 - C_2 = 0$, for different values of the intercavity coupling κ , and for different intensities of the driving field (i.e., by varying ϵ) in both linear ($BI_1/C_2 \ll 1$) and nonlinear ($BI_1/C_2 \approx 1$) regimes [for details regarding the nonlinearity condition,

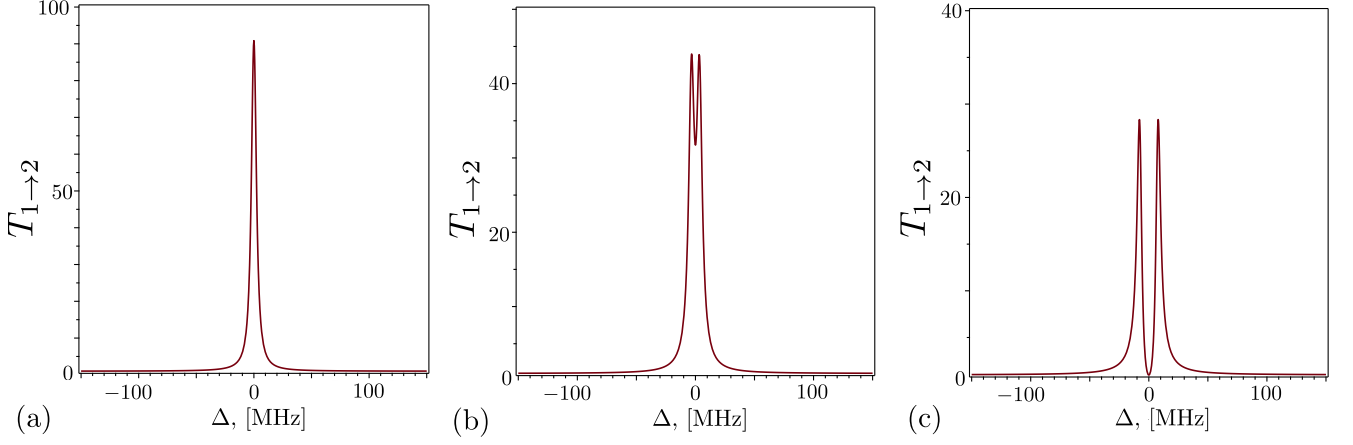


FIG. 12. Transmission spectrum $T_{1 \rightarrow 2}$ when there is a coupling between the microresonators R_1 and R_2 for: (a) $A = 21$ MHz, $\kappa = 1$ MHz; (b) $A = 24$ MHz, $\kappa = 4$ MHz; and (c) $A = 25.5$ MHz, $\kappa = 8$ MHz. The power of the input signal is $P = 100$ nW. This figure qualitatively reproduces the experimentally-obtained Fig. S6 in Ref. [17].

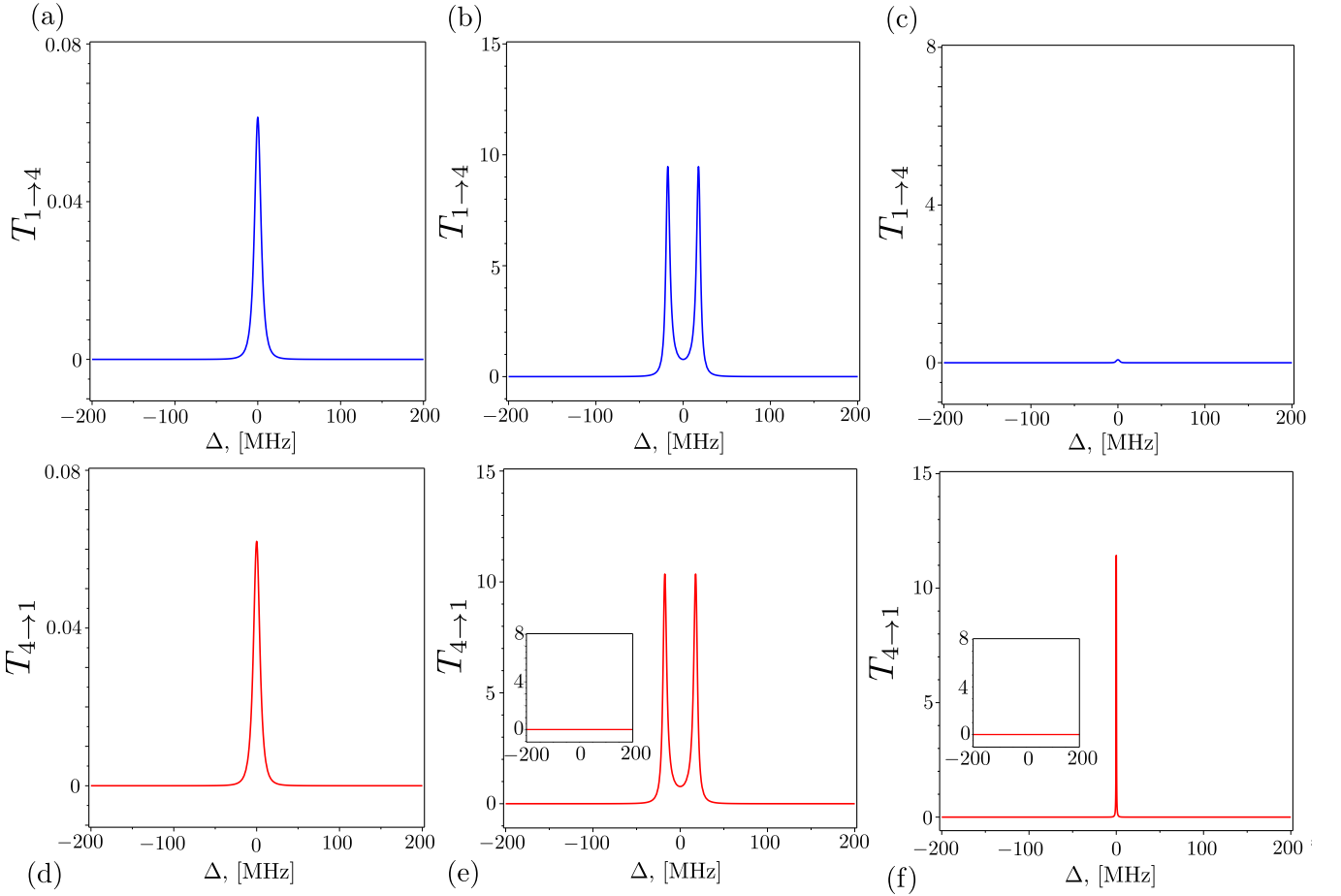


FIG. 13. Transmission spectrum $T_{1 \rightarrow 4}$ [$T_{4 \rightarrow 1}$] versus detuning $\Delta = \omega - \omega_c$ for: (a) [(d)] no amplification $A = 0$ MHz, $\kappa = 1$ MHz; (b) [(e)] $A = 25$ MHz, $\kappa = 20$ MHz; (c) [(f)] $A = 25$ MHz, $\kappa = 0.2$ MHz. The power of the input signal is $P = 1$ μ W. Graphs (c) and (f) clearly show non-reciprocity of light propagation. The insets of panels (e) and (f) show the spectra assuming no input signal. This figure qualitatively reproduces the experimentally-obtained Fig. 4 in Ref. [17].

see Eq. (22)]. One can observe an increasing spectral line broadening of the transmitted light for stronger driving

fields ϵ in the nonlinear regime, indicating rising losses due to the gain saturation for small values of κ [green

dashed and blue dash-dotted curves in Fig. 9(a)]. Moreover, the transmission spectra in Figs. 9(b) and 9(c) display a squared Lorentzian line shape, which is characteristic for EPs [39–41]. Also, in the nonlinear case, the splitting of the supermodes occurs for larger $\kappa > \kappa_{\text{EP}}$ and more intensive fields [Figs. 9(b), 9(c)]. A similar behavior is observed in the transmission spectrum $T_{4 \rightarrow 1}$.

IV. A COMPARISON WITH EXPERIMENTAL RESULTS OF REF. [17]

For simplicity, when plotting the graphs in this section, we assume that the losses in both cavities are comprised mainly by the losses due to the coupling of the cavities to the waveguides $\Gamma_i = C_i + \gamma_i = \gamma_i$, $i = 1, 2$, i.e., we set the intrinsic losses C_i to zero. The latter assumption also implies that the system considered has a broken \mathcal{PT} -symmetry, i.e., $A - C_1 - C_2 \neq 0$, according to Eq. (20). At the same time, the total losses in the system are expected to be larger than the gain, i.e., $(A - \gamma_1 - \gamma_2) < 0$. Also, the active microcavity is assumed to operate near the threshold $A \approx \gamma_1 > \gamma_2$.

In this section, we discuss possible applications of the semiclassical Scully-Lamb laser theory in the prediction of some nontrivial light behavior that was experimentally observed in Refs. [17, 18]. In those papers, the authors experimentally studied a system of coupled \mathcal{PT} -symmetric whispering-gallery microcavities, i.e., a system that is identical to that presented in Fig. 1 and which is the focus of the theoretical study of this manuscript. Below, we theoretically reproduce some of the experimental graphs of Ref. [17] in a qualitative rather than quantitative way (meaning that we make some additional assumptions regarding the system parameters, used in constructing the graphs here). Nevertheless, as was just mentioned, a qualitative comparison can be made, and positive conclusions can be inferred regarding the applicability of the Scully-Lamb laser model, in its semiclassical limit, to explain some of the results of Ref. [17]. We note that in the construction of the graphs shown here, which are presented in Figs. 10–13, we do *not* invoke \mathcal{PT} -symmetry in the system (see also the text below).

For clarity, in the captions of some of our figures we indicate the corresponding experimental plots of Ref. [17] that we try to theoretically reproduce. Also, in order to stress the similarity between the figures reproduced here and the original experimental graphs of Ref. [17], we keep the axis scales of the plots to be the same as those given in Ref. [17].

For example, in Fig. 10, which corresponds to the experimentally-obtained Fig. 1(f) in Ref. [17], the transmission spectrum $T_{1 \rightarrow 2}$ is shown when only the WG1 and the microresonator R_1 are coupled in the system and $\kappa = 0$, i.e., only the first resonator is considered. Thus, by coupling the signal sent from port 1 to the active cavity, one obtains a substantial signal amplification, when detecting the output signal at port 2. In this case, the

active cavity just enhances the incoming field. The inset of Fig. 10 demonstrates that amplification does not occur if there is no input signal.

In Fig. 11, which corresponds to the experimentally-obtained Fig. 3 in Ref. [17], we show the transmission spectra for the light propagating in the directions $1 \rightarrow 4$ and $4 \rightarrow 1$ in the linear regime, i.e., the laser cavity is assumed to be below the lasing threshold $A < \gamma_1$. One can see the linear response of the propagating signal when the inter-cavity coupling coefficient κ is lower or larger than κ_{cr} , where κ_{cr} denotes the critical point, when the supermodes start splitting. We note that, in Fig. 11, a linear behavior of the transmitted light is already observed in the unbalanced gain-loss regime, i.e., when \mathcal{PT} -symmetry is broken in the system.

Figure 12, which corresponds to the experimentally-obtained Fig. S6 in Ref. [17], displays the transmitted spectrum $T_{1 \rightarrow 2}$ versus the detuning $\Delta = \omega - \omega_c$, for various values of the gain A and the intercavity coupling κ . One can see the appearance of the supermodes splitting in the system with the increasing values of κ . Conversely, for smaller values of κ , the two supermodes coalesce resulting in only one peak in the spectrum.

Non-reciprocity of light propagation

Here, to complement Sec. III D, we further discuss the theoretical microscopic prediction of non-reciprocity of the propagating light in the considered coupled active-passive microresonators system as shown Fig. 13, which corresponds to the experimentally-obtained Fig. 4 in Ref. [17]. It is seen that there is an enhancement in the transmitted light from port 4 to port 1, and tending to zero transmission $T_{1 \rightarrow 4}$ in the opposite direction for small values of κ . Meaning that the system starts behaving nonreciprocally. The latter nonlinear effect was observed in Ref. [17], but, naturally, could not be explained based on the used linear rate equations there. *Utilizing the semiclassical laser theory, one can attain the needed nonlinear term arising from the laser gain saturation in the active microcavity. Moreover, this non-reciprocity is observed without invoking \mathcal{PT} -symmetry*, because it can be already observed when the gain and loss are unbalanced in the system (see Fig. 13). The inset of Fig. 13(f) indicates that the observed nonlinearity is not caused by the lasing initiated by spontaneous emission in the active cavity.

V. CONCLUSIONS

We have applied the quantum Scully-Lamb laser theory to a pair of \mathcal{PT} -symmetric coupled whispering-gallery microcavities, i.e., a system, which consists of both active and passive microring cavities, such that gain and losses are balanced in the system. It has been shown that, in the nonlinear regime, or more precisely, under

the condition in which the gain saturation in the active cavity is comparable to the losses in the passive cavity, the intense intracavity fields of the steady state lead to the modification of the eigenmodes and of the EPs of the \mathcal{PT} -symmetric system. Namely, the imaginary part of the eigenspectrum acquires an extra negative term due to the gain saturation effects. This effect leads to the shift of the EP either to lower or larger values depending on the gain saturation B and the propagation direction of the driving fields. Starting from the master equation for this coupled system, including dissipation, gain, and gain saturation, and applying the semiclassical approximation, we are able to describe the experimental results obtained in Refs. [17, 18]. In particular, this approach is able to reproduce the observed non-reciprocal light propagation in the coupled system of whispering-gallery microcavities. We have also shown that the gain saturation mechanism in the active cavity is crucial for the observation of light non-reciprocity. Moreover, we have found that the unidirectional light propagation can be observed even when the \mathcal{PT} -symmetry condition is not fulfilled. It should be stressed that neither \mathcal{PT} -symmetry nor its breaking is required for nonreciprocity. The nonreciprocity observed in our system is a result of a nonlinearity and, in the broken \mathcal{PT} -regime, such nonlinearity can be observed at much lower input intensity.

In summary, we proposed, applied, and validated the Scully-Lamb laser model, with the non-Lindbladian master equation, for coupled resonators with losses, gain, and gain saturation. Although we studied non-reciprocity and exceptional points applying the semiclassical approximation, this master equation allows for a quantum description of the cavity fields. This approach constitutes a promising tool for the study of quantum optical effects in coupled resonators with balanced (or unbalanced) gain and losses.

ACKNOWLEDGMENTS

I.I.A. was supported by Grant Agency of the Czech Republic (Project No. 17-23005Y), the Project CZ.02.1.010.00.016.0190000754, and the Project LO1305 of the Ministry of Education, Youth and Sports of the Czech Republic. A.M. and F.N. acknowledge the support of a grant from the John Templeton Foundation. F.N. is supported in part by the: MURI Center for Dynamic Magneto-Optics via the Air Force Office of Scientific Research (AFOSR) (FA9550-14-1-0040), Army Research Office (ARO) (Grant No. 73315PH), Asian Office of Aerospace Research and Development (AOARD) (Grant No. FA2386-18-1-4045), Japan Science and Technology Agency (JST) (the Q-LEAP program, and CREST Grant No. JPMJCR1676), Japan Society for the Promotion of Science (JSPS) (JSPS-RFBR Grant No. 17-52-50023), and the RIKEN-AIST Challenge Research Fund. S.S. is supported in part by the Army Research Office (ARO) (Grant No. W911NF1910065). S.K.O. is supported by

Army Research Office (ARO) grant No. W911NF-18-1-0043, Air Force Office of Scientific Research (AFOSR) award No. FA9550-18-1-0235, National Science Foundation (NSF) (1807485), and by The Pennsylvania State University, Materials Research Institute (MRI).

Appendix A: Derivation of the master equation in Eq. (2)

To make this article self-consistent, in this Appendix, we present a derivation of the quantum laser master equation, given in Eq. (2), for the Scully-Lamb laser model based on the derivation of Yamamoto and Imamoğlu Ref. [36]. This derivation bears a phenomenological character and, as such, naturally allows to incorporate all the terms of the interaction Hamiltonian of the fields without the need to solve the Schrödinger equation directly. Another derivation of the master equation (2) can be found in Ref. [37].

The active cavity is represented by a general four-level laser system in which the two intermediate energy levels are coupled by the laser mode (see Fig. 14). In this limit, the uppermost level of the atom may be adiabatically eliminated to give an effective three-level system. The latter assumption is valid as long as the decay rate from the uppermost state $|1\rangle$ to the upper laser level $|e\rangle$ is much faster than all other rates in the atom-field system. In this limit, one has an effective incoherent pumping rate r from the atomic ground state $|0\rangle$ into $|e\rangle$. Additionally, the laser mode in the active cavity is coupled to the passive microresonator.

The interaction Hamiltonian \hat{H}_I , describing such two coupled active-passive microresonators system, is given by

$$\hat{H}_I = ig \left(\hat{\sigma}_+ \hat{a}_1 - \hat{\sigma}_- \hat{a}_1^\dagger \right) + i\kappa \left(\hat{a}_1 \hat{a}_2^\dagger - \hat{a}_1^\dagger \hat{a}_2 \right). \quad (\text{A1})$$

Specifically, the second term in Eq. (A1) describes the linear interaction between the modes in the active (a_1) and passive (a_2) resonators; while the first term describes the interaction between the mode a_1 with only two levels ($|g\rangle$ and $|e\rangle$) within the standard Jaynes-Cummings model. The operators $\hat{\sigma}_k$, $k = +, -$, are spin-raising and spin-lowering operators of the atom in the active medium, respectively. The constants g , κ denote the coupling strength between the atom and the field in the laser cavity, and between the two fields propagating in two different cavities, respectively. We also assumed that the atomic and active cavity field resonances coincide.

The quantum Liouville equation for the density operator $\hat{\rho}$ in the interaction picture, which describes the atom-field-field dynamics is:

$$\frac{d}{dt} \hat{\rho} = \frac{1}{i\hbar} \left[\hat{H}_I, \hat{\rho} \right]. \quad (\text{A2})$$

In the active cavity, the optical gain is provided by the excited atoms, which are pumped by an external field. The

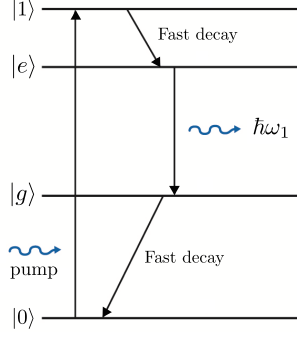


FIG. 14. Four-level atom laser scheme in an active microresonator.

interaction between the atom and an external pumping field, that provides an inverse population in our effective three-level atom laser (depicted in Fig. 14), can be described by the following equation

$$\frac{d}{dt}\hat{\rho} = -\frac{r}{2}(\hat{\sigma}_{00}\hat{\rho} + \hat{\rho}\hat{\sigma}_{00} - 2\hat{\sigma}_{e0}\hat{\rho}\hat{\sigma}_{0e}), \quad (\text{A3})$$

where $\hat{\sigma}_{00} = \hat{\sigma}_{0e}\hat{\sigma}_{e0}$, and $\hat{\sigma}_{0e}$ ($\hat{\sigma}_{e0}$) is the spin operator for the atomic transition from $|0\rangle$ ($|e\rangle$) to $|e\rangle$ ($|0\rangle$). The coefficient r accounts for the pumping rate of the atom.

To include spontaneous emission and the emission caused by external dephasing processes into an external reservoir field, we need to add in Eq. (A2) the following terms:

$$\begin{aligned} \frac{d}{dt}\hat{\rho} = & -\frac{\gamma_{\text{sp}}}{2}(\hat{\sigma}_+\hat{\sigma}_-\hat{\rho} + \hat{\rho}\hat{\sigma}_+\hat{\sigma}_- - 2\hat{\sigma}_-\hat{\rho}\hat{\sigma}_+) \\ & -\frac{\gamma_d}{2}(\hat{\sigma}_{ee}\hat{\rho}\hat{\sigma}_{gg} + \hat{\sigma}_{gg}\hat{\rho}\hat{\sigma}_{ee}), \end{aligned} \quad (\text{A4})$$

where γ_{sp} and γ_d are, respectively, the rates of spontaneous emission, and the emission imposed by additional dephasing processes.

Now, collecting together Eqs. (A2)–(A4), one arrives at the master equation for the density operator $\hat{\rho}$

$$\begin{aligned} \frac{d}{dt}\hat{\rho} = & \frac{1}{i\hbar}[\hat{H}_I, \hat{\rho}] - \frac{1}{2}\sum_{i=1}^2 C_i \hat{L}_i^d(\hat{\rho}) \\ & -\frac{r}{2}(\hat{\sigma}_{00}\hat{\rho} + \hat{\rho}\hat{\sigma}_{00} - 2\hat{\sigma}_{e0}\hat{\rho}\hat{\sigma}_{0e}) \\ & -\frac{\gamma_{\text{sp}}}{2}(\hat{\sigma}_+\hat{\sigma}_-\hat{\rho} + \hat{\rho}\hat{\sigma}_+\hat{\sigma}_- - 2\hat{\sigma}_-\hat{\rho}\hat{\sigma}_+) \\ & -\frac{\gamma_d}{2}(\hat{\sigma}_{ee}\hat{\rho}\hat{\sigma}_{gg} + \hat{\sigma}_{gg}\hat{\rho}\hat{\sigma}_{ee}), \end{aligned} \quad (\text{A5})$$

where we introduced a Lindbladian damping super operator as $\hat{L}_i^d(\hat{O}) = \hat{a}_i^\dagger \hat{a}_i \hat{O} + \hat{O} \hat{a}_i^\dagger \hat{a}_i - 2\hat{a}_i \hat{O} \hat{a}_i^\dagger$.

To obtain the master equation for the reduced field density operator $\hat{\rho}_f$, which describes the dynamics of the optical fields in the cavities, one has to trace out the density operator $\hat{\rho}$ in Eq. (A5) over the atom states. Namely,

$$\frac{d}{dt}\hat{\rho}_f = \text{Tr}_a \left[\frac{d}{dt}\hat{\rho} \right] = \sum_{i=0,e,g} \left\langle i \left| \frac{d}{dt}\hat{\rho} \right| i \right\rangle. \quad (\text{A6})$$

$$\begin{aligned} \frac{d}{dt}\hat{\rho}_f = & \frac{1}{i\hbar}[\hat{H}_f, \hat{\rho}_f] - \frac{1}{2}\sum_{i=1}^2 C_i \hat{L}_i^d(\hat{\rho}_f) \\ & + g(\hat{a}_1 \hat{\rho}_{ge} - \hat{a}_1^\dagger \hat{\rho}_{eg} - \rho_{ge} \hat{a}_1 + \rho_{eg} \hat{a}_1^\dagger), \end{aligned} \quad (\text{A7})$$

where the Hamiltonian H_f accounts for the field interaction between active and passive cavities, i.e., it is the second term in Eq. (A1). The operator $\hat{\rho}_{ge} = \langle g | \frac{d}{dt}\hat{\rho} | e \rangle$, from Eq. (A5), obeys the following equation

$$\frac{d}{dt}\hat{\rho}_{ge} = g(\hat{\rho}_{gg}\hat{a}_1^\dagger - \hat{a}_1^\dagger \hat{\rho}_{ee}) - \frac{\gamma_T}{2}\hat{\rho}_{ge}, \quad (\text{A8})$$

where $\gamma_T = \gamma_{\text{sp}} + \gamma_d$ is the total decay rate of the atom. The same relation, given in Eq. (A8), also holds true for the operator $\hat{\rho}_{eg} = \langle e | \hat{\rho} | g \rangle$.

Assuming $\gamma_T \gg C_1, C_2, \kappa$, one eliminates $\hat{\rho}_{ge}$ and $\hat{\rho}_{eg}$ in the adiabatic approximation, i.e., $\frac{d}{dt}\hat{\rho}_{ge} = 0$. Thus, one obtains

$$\hat{\rho}_{ge} = \frac{2g}{\gamma_T}(\hat{\rho}_{gg}\hat{a}_1^\dagger - \hat{a}_1^\dagger \hat{\rho}_{ee}) \quad (\text{A9})$$

Substituting $\hat{\rho}_{ge}$ and $\hat{\rho}_{eg}$ in Eq. (A7) one obtains

$$\begin{aligned} \frac{d}{dt}\hat{\rho}_f = & \frac{1}{i\hbar}[\hat{H}_f, \hat{\rho}_f] - \frac{1}{2}\sum_{i=1}^2 C_i \hat{L}_i^d(\hat{\rho}_f) \\ & - \frac{2g^2}{\gamma_T} \left(\hat{L}_1^d(\hat{\rho}_{gg}) + \hat{L}_1^a(\hat{\rho}_{ee}) \right), \end{aligned} \quad (\text{A10})$$

where $L_i^a(\hat{O}) = \hat{a}_i \hat{a}_i^\dagger \hat{O} + \hat{O} \hat{a}_i \hat{a}_i^\dagger - 2\hat{a}_i^\dagger \hat{O} \hat{a}_i$ is the Lindbladian amplification super operator.

Moreover, $\hat{\rho}_{ee}$ and $\hat{\rho}_{gg}$ satisfy the following equations

$$\begin{aligned} \frac{d}{dt}\hat{\rho}_{ee} = & \frac{2g^2}{\gamma_T} - \gamma_{\text{sp}}\hat{\rho}_{ee} + r\hat{\rho}_{00}, \\ \frac{d}{dt}\hat{\rho}_{gg} = & -\frac{2g^2}{\gamma_T}\hat{L}_1^d(\hat{\rho}_{gg}) + \gamma_{\text{sp}}\hat{\rho}_{ee}. \end{aligned} \quad (\text{A11})$$

If the population of the lower energy level $|g\rangle$ is very low, i.e., the energy quickly decays into the ground state $|0\rangle$, and if the gain saturation is weak, then one may write

$$\hat{\rho}_{gg} \simeq 0, \quad \text{and} \quad \hat{\rho}_{00} \simeq \hat{\rho}_f, \quad (\text{A12})$$

Applying standard perturbation techniques to Eq. (A11), one arrives at

$$\hat{\rho}_{ee} \simeq \frac{r}{\gamma_{\text{sp}}}\hat{\rho}_f - \frac{2g^2 r}{\gamma_T \gamma_{\text{sp}}^2} \left(\hat{a}_1 \hat{a}_1^\dagger \hat{\rho}_f + \hat{\rho}_f \hat{a}_1 \hat{a}_1^\dagger \right). \quad (\text{A13})$$

Combining now Eqs. (A12), (A13), and Eq. (A10), one attains the master equation for the two field operator in the interaction picture

$$\begin{aligned} \frac{d}{dt}\hat{\rho}_f = & \frac{1}{i\hbar}[\hat{H}_f, \hat{\rho}_f] - \frac{A}{2}\hat{L}_1^a(\hat{\rho}_f) - \frac{1}{2}\sum_{i=1}^2 C_i \hat{L}_i^d(\hat{\rho}_f) \\ & + \frac{B}{2} \left[(\hat{a}_1 \hat{a}_1^\dagger)^2 \hat{\rho}_f + 2\hat{a}_1 \hat{a}_1^\dagger \hat{\rho}_f \hat{a}_1 \hat{a}_1^\dagger + \hat{\rho}_f (\hat{a}_1 \hat{a}_1^\dagger)^2 \right. \\ & \left. - 2\hat{a}_1^\dagger \hat{\rho}_f \hat{a}_1 \hat{a}_1^\dagger \hat{a}_1 - 2\hat{a}_1^\dagger \hat{a}_1 \hat{a}_1^\dagger \hat{\rho}_f \hat{a}_1 \right], \end{aligned} \quad (\text{A14})$$

with

$$A = \frac{4g^2r}{\gamma_T\gamma_{sp}}, \quad B = \frac{A^2}{2r}, \quad (\text{A15})$$

where the coefficient A stands for the linear gain, and B is the gain saturation coefficient.

For the case of the ideal laser system with $\Gamma_e = \Gamma_g = \Gamma$ and $\gamma_{\text{dep}} = \Gamma_{eg} = 0$, one attains the quantum laser master equation within the Scully-Lamb laser theory. In the weakly saturated regime, the spontaneous emission on the laser transition can be discarded, and one obtains

$$\begin{aligned} \hat{\rho}_{gg} &\simeq \frac{2g^2}{\Gamma^2} \hat{a}_1^\dagger \hat{\rho}_{ee} \hat{a}_1 = \frac{2rg^2}{\Gamma^3} \hat{a}_1^\dagger \hat{\rho}_f \hat{a}_1, \\ \hat{\rho}_{ee} &\simeq \frac{r}{\Gamma} \hat{\rho}_f - \frac{rg^2}{\Gamma^3} \left[\hat{a}_1 \hat{a}_1^\dagger \hat{\rho}_f + \hat{\rho}_f \hat{a}_1 \hat{a}_1^\dagger \right]. \end{aligned} \quad (\text{A16})$$

Substituting equations in Eqs. (A16) into Eq. (A10), we obtain

$$\begin{aligned} \frac{d}{dt} \hat{\rho}_f &= \frac{1}{i\hbar} \left[\hat{H}_f, \hat{\rho}_f \right] - \frac{A}{2} \hat{L}_1^a(\hat{\rho}_f) - \frac{1}{2} \sum_{i=1}^2 C_i \hat{L}_i^d(\hat{\rho}_f) \\ &+ \left[\frac{B}{8} \left\{ \hat{\rho}_f (\hat{a}_1 \hat{a}_1^\dagger)^2 + 3\hat{a}_1 \hat{a}_1^\dagger \hat{\rho}_f \hat{a}_1 \hat{a}_1^\dagger - 4\hat{a}_1^\dagger \hat{\rho}_f \hat{a}_1 \hat{a}_1^\dagger \hat{a}_1 \right\} + \text{h.c.} \right], \end{aligned} \quad (\text{A17})$$

where the gain and gain saturation coefficients are now expressed as

$$A = \frac{2g^2r}{\Gamma^2}, \quad \text{and} \quad B = \frac{4g^2}{\Gamma^2} A. \quad (\text{A18})$$

Note a typo in the prefactor of the gain saturation coefficient B in Eq. (A18) in Ref. [36]. Namely, there is a prefactor 1, instead of 4.

We may also add the Hamiltonian term related to the coupling between the cavity field \hat{a}_1 and the external driving coherent classical field into the master equation. Such a Hamiltonian can be given by

$$\hat{H}_{\text{drv}} = i\epsilon \left[\hat{a}_1 \exp(i\omega_l t) - \hat{a}_1^\dagger \exp(-i\omega_l t) \right], \quad (\text{A19})$$

where the coupling constant $\epsilon \equiv \sqrt{\gamma_1 P / (\hbar\omega_l)}$ accounts for the coupling between the driving external coherent field with power \mathcal{P} and the cavity field \hat{a}_1 .

By rewriting the field Hamiltonian \hat{H}_f in the Schrödinger picture, we finally arrive at Eq. (2).

Appendix B: Derivation of Eq. (23), and some exact formulas from Sec. III E

Working in the reference frame where the phase of the driving field is zero, and by expressing the complex amplitudes in the rate equations in Eq. (10) as $A_k = |A_k| e^{i\phi_k}$, one obtains the following equations for the steady-state:

$$\begin{aligned} i\Delta |A_1| + \frac{G_1}{2} |A_1| - \kappa |A_2| e^{i(\phi_2 - \phi_1)} - \frac{B}{2} |A_1|^3 - \epsilon e^{-i\phi_1} &= 0, \\ i\Delta |A_2| - \frac{\Gamma_2}{2} |A_2| + \kappa |A_1| e^{-i(\phi_2 - \phi_1)} &= 0. \end{aligned} \quad (\text{B1})$$

Replacing now $|A_2| \exp[i(\phi_2 - \phi_1)]$ by $|A_1|$ in the second equation of Eq. (B1) and inserting it into the first equation, we attain

$$\left(i\Delta + \frac{G_1}{2} - \frac{2\kappa^2}{\Gamma_2 - 2i\Delta} \right) |A_1| - \frac{B}{2} |A_1|^3 - \epsilon \exp(-i\phi_1) = 0. \quad (\text{B2})$$

Separating the real and imaginary parts in Eq. (B2) and equalizing them to zero, one arrives at

$$\begin{aligned} \cos \phi_1 &= \frac{|A_1|}{2\epsilon} (G_1 - f\Gamma_2 - B|A_1|^2), \\ \sin \phi_1 &= \frac{|A_1|\Delta}{\epsilon} (f - 1). \end{aligned} \quad (\text{B3})$$

where f is given in Eq. (24). Utilizing now the standard trigonometric relation $\cos^2 \phi_1 + \sin^2 \phi_1 = 1$, and collecting together the coefficients at each order of the real amplitude, we finally obtain the cubic equation for the field intensity $I_1 = |A_1|^2$, given in Eq. (23).

The unique real solution of the steady-state intensity I_1 , given in Eq. (23), is

$$I_1 = \frac{1}{6\lambda_1 x} \left[x^2 - 2\lambda_2 x + 4\lambda_2^2 - 12\lambda_1 \lambda_3 \right], \quad (\text{B4})$$

where

$$\begin{aligned} x^3 &= 12\sqrt{3} \left(27\lambda_1^2 \lambda_4^2 - 18\lambda_1 \lambda_2 \lambda_3 \lambda_4 + 4\lambda_1 \lambda_3^3 + 4\lambda_1^3 \lambda_4 \right. \\ &\left. - \lambda_2^2 \lambda_3^2 \right)^{1/3} + 36\lambda_1 \lambda_2 \lambda_3 - 108\lambda_1^2 \lambda_4 - 8\lambda_2^3, \end{aligned} \quad (\text{B5})$$

with the coefficients λ_k introduced in Eq. (24). For the transmission spectra $T_{4 \rightarrow 1}$, given in Eq. (27), the steady-state intensity I_1 has the same solution as in Eq. (B4), and with the same coefficients λ_k in Eq. (24), except the coefficient λ_4 , which reads now as

$$\lambda_4 = -f\epsilon^2. \quad (\text{B6})$$

By combining together the input-output relation $A_{\text{out}} = A_{\text{in}} + \sqrt{\gamma_1} A_1$ with the solution for the phase of the complex amplitude A_1 in Eq. (B3), one can straightforwardly find the transmission spectrum $T_{1 \rightarrow 2}$, after applying Eq. (25), as follows

$$T_{1 \rightarrow 2} = 1 + \frac{2\gamma_1 I_1}{\epsilon^2} \left(\frac{\gamma_1}{2} - F \right) - \frac{\gamma_1 B I_1^2}{\epsilon^2}, \quad (\text{B7})$$

where F is given in Eq. (24).

- [1] C. M. Bender and S. Boettcher, “Real spectra in non-Hermitian Hamiltonians having \mathcal{PT} symmetry,” *Phys. Rev. Lett.* **80**, 5243–5246 (1998).
- [2] C. M. Bender, “Making sense of non-Hermitian Hamiltonians,” *Rep. Prog. Phys.* **70**, 947–1018 (2007).
- [3] C. M. Bender, D. C. Brody, and H. F. Jones, “Must a Hamiltonian be Hermitian?” *Am. J. Phys.* **71**, 1095–1102 (2003).
- [4] R. El-Ganainy, K. G. Makris, D. N. Christodoulides, and Z. H. Musslimani, “Theory of coupled optical \mathcal{PT} -symmetric structures,” *Opt. Lett.* **32**, 2632 (2007).
- [5] K. G. Makris, R. El-Ganainy, D. N. Christodoulides, and Z. H. Musslimani, “Beam dynamics in \mathcal{PT} symmetric optical lattices,” *Phys. Rev. Lett.* **100**, 103904 (2008).
- [6] L. Feng, R. El-Ganainy, and L. Ge, “Non-Hermitian photonics based on parity-time symmetry,” *Nat. Photon.* **11**, 752 (2017).
- [7] R. El-Ganainy, K. G. Makris, M. Khajavikhan, Z. H. Musslimani, S. Rotter, and D. N. Christodoulides, “Non-Hermitian physics and \mathcal{PT} symmetry,” *Nat. Phys.* **14**, 11 (2018).
- [8] M. Miri and A. Alu, “Exceptional points in optics and photonics,” *Science* **363**, 7709 (2019).
- [9] Ş. K. Özdemir, S. Rotter, F. Nori, and L. Yang, “Parity-time symmetry and exceptional points in photonics,” *Nature Materials*, in press (2019).
- [10] Z.-P. Liu, J. Zhang, Ş. K. Özdemir, B. Peng, H. Jing, X.-Y. Lü, C.-W. Li, L. Yang, F. Nori, and Y.-X. Liu, “Metrology with \mathcal{PT} -symmetric cavities: Enhanced sensitivity near the \mathcal{PT} -phase transition,” *Phys. Rev. Lett.* **117**, 110802 (2016).
- [11] W. Chen, Ş. K. Özdemir, G. Zhao, J. Wiersig, and L. Yang, “Exceptional points enhance sensing in an optical microcavity,” *Nature (London)* **548**, 192 (2017).
- [12] H. Hodaei, U. H. Absar, S. Wittek, H. Garcia-Gracia, R. El-Ganainy, D. N. Christodoulides, and M. Khajavikhan, “Enhanced sensitivity at higher-order exceptional points,” *Nature (London)* **548**, 187 (2017).
- [13] Z. Lin, H. Ramezani, T. Eichelkraut, T. Kottos, H. Cao, and D. N. Christodoulides, “Unidirectional invisibility induced by \mathcal{PT} -symmetric periodic structures,” *Phys. Rev. Lett.* **106**, 213901 (2011).
- [14] A. Regensburger, C. Bersch, M.-A. Miri, G. Onishchukov, D. N. Christodoulides, and U. Peschel, “Parity-time synthetic photonic lattices,” *Nature (London)* **488**, 167 (2012).
- [15] L. Feng, Z. J. Wong, R.-M. Ma, Y. Wang, and X. Zhang, “Single-mode laser by parity-time symmetry breaking,” *Science* **346**, 972 (2014).
- [16] H. Hodaei, M.-A. Miri, M. Heinrich, D. N. Christodoulides, and M. Khajavikhan, “Parity-time-symmetric microring lasers,” *Science* **346**, 975 (2014).
- [17] B. Peng, Ş. K. Özdemir, F. Lei, F. Monifi, M. Gianfreda, G. L. Long, S. Fan, F. Nori, C. Bender, and L. Yang, “Parity-time-symmetric whispering-gallery microcavities,” *Nat. Phys.* **10**, 394 (2014).
- [18] L. Chang, X. Jiang, S. Hua, C. Yang, J. Wen, L. Jiang, G. Li, G. Wang, and M. Xiao, “Parity-time symmetry and variable optical isolation in active-passive-coupled microresonators,” *Nat. Photon.* **8**, 524 (2014).
- [19] M. Brandstetter, M. Liertzer, C. Deutsch, P. Klang, J. Schoberl, H. E. Tureci, G. Strasser, K. Unterrainer, and S. Rotter, “Reversing the pump dependence of a laser at an exceptional point,” *Nat. Commun.* **5**, 4034 (2014).
- [20] B. Peng, Ş. K. Özdemir, S. Rotter, H. Yilmaz, M. Liertzer, F. Monifi, C. M. Bender, F. Nori, and L. Yang, “Loss-induced suppression and revival of lasing,” *Science* **346**, 328 (2014).
- [21] H. Jing, Ş. K. Özdemir, X.-Y. Lü, J. Zhang, L. Yang, and F. Nori, “ \mathcal{PT} -symmetric phonon laser,” *Phys. Rev. Lett.* **113**, 053604 (2014).
- [22] H. Lü, Ş. K. Özdemir, L. M. Kuang, F. Nori, and H. Jing, “Exceptional points in random-defect phonon lasers,” *Phys. Rev. App.* **8**, 044020 (2017).
- [23] J. Schindler, A. Li, M.C. Zheng, F. M. Ellis, and T. Kottos, “Experimental study of active LRC circuits with \mathcal{PT} symmetries,” *Phys. Rev. A* **84**, 040101(R) (2011).
- [24] H. Xu, D. Mason, L. Jiang, and J. G. E. Harris, “Topological energy transfer in an optomechanical system with exceptional points,” *Nature (London)* **537**, 80 (2016).
- [25] H. Jing, Ş. K. Özdemir, H. Lü, and F. Nori, “High-order exceptional points in optomechanics,” *Scientific Reports* **7**, 3386 (2017).
- [26] X. Zhu, H. Ramezani, C. Shi, J. Zhu, and X. Zhang, “ \mathcal{PT} -symmetric acoustics,” *Phys. Rev. X* **4**, 031042 (2014).
- [27] R. Fleury, D. Sounas, and A. Alu, “An invisible acoustic sensor based on parity-time symmetry,” *Nat. Commun.* **6**, 5905 (2015).
- [28] H. Benisty, A. Degiron, A. Lupu, A. De Lustrac, S. Chenais, S. Forget, M. Besbes, G. Barbillon, A. Bruyant, S. Blaize, and G. Lerondel, “Implementation of \mathcal{PT} symmetric devices using plasmonics: principle and applications,” *Optics Express* **19**, 18004 (2011).
- [29] M. Kang, F. Liu, and J. Li, “Effective spontaneous \mathcal{PT} -symmetry breaking in hybridized metamaterials,” *Phys. Rev. A* **87**, 053824 (2013).
- [30] F. Quijandria, U. Naether, Ş. K. Özdemir, F. Nori, and D. Zueco, “ \mathcal{PT} -symmetric circuit QED,” *Phys. Rev. A* **97**, 053846 (2018).
- [31] K. Kawabata, Y. Ashida, and M. Ueda, “Information retrieval and criticality in parity-time-symmetric systems,” *Phys. Rev. Lett.* **119**, 190401 (2017).
- [32] Y. Ashida, S. Furukawa, and M. Ueda, “Parity-time symmetric quantum critical phenomena,” *Nat. Commun.* **8**, 15791 (2017).
- [33] T. Liu, Y.-R. Zhang, Q. Ai, Z. Gong, K. Kawabata, M. Ueda, and F. Nori, “Second-order topological phases in non-Hermitian systems,” *Phys. Rev. Lett.* **122**, 076801 (2019).
- [34] H. Ramezani, T. Kottos, R. El-Ganainy, and D. N. Christodoulides, “Unidirectional nonlinear \mathcal{PT} -symmetric optical structures,” *Phys. Rev. A* **82**, 043803 (2010).
- [35] M. Sargent III, M. Scully, and W. Lamb Jr., *Laser Physics* (Westview Press, 1974).
- [36] Y. Yamamoto and A. Imamoglu, *Mesoscopic Quantum Optics* (John Wiley and Sons, New York, 1999).

- [37] M. Orszag, *Quantum Optics* (Springer, Berlin, 2008).
- [38] J. Gea-Banacloche, “Emergence of classical radiation fields through decoherence in the Scully-Lamb laser model,” *Found. Phys.* **28**, 531 (1997).
- [39] G. Yoo, H.-S. Sim, and H. Schomerus, “Quantum noise and mode nonorthogonality in non-Hermitian \mathcal{PT} -symmetric optical resonators,” *Phys. Rev. A* **84**, 063833 (2011).
- [40] W. R. Sweeney, C. W. Hsu, S. Rotter, and A. D. Stone, “Perfectly absorbing exceptional points and chiral absorbers,” [arXiv:1807.08805](https://arxiv.org/abs/1807.08805) (2018).
- [41] A. Pick, B. Zhen, O. D. Miller, C. W. Hsu, F. Hernandez, A. W. Rodriguez, M. Soljačić, and S. G. Johnson, “General theory of spontaneous emission near exceptional points,” *Opt. Express* **25**, 12325 (2017).